3

Thermal Diffusivity of Ceramics During Neutron Irradiation

Masafumi Akiyoshi[1], Hidetsugu Tsuchida[1] and Toyohiko Yano[2]
[1]*Department of Nuclear Engineering, Kyoto University, Yoshida-Honmachi, Sakyo-ku, Kyoto*
[2]*Research Laboratory for Nuclear Reactors, Tokyo Institute of Technology, O-okayama, Meguro, Tokyo*
Japan

1. Introduction

Several structural ceramic materials possess many superior properties for nuclear applications, such as blanket of future fusion reactor or core material of high-temperature gas cooling fission reactor for hydrogen generation, where they would be exposed to high fluence of neutrons at temperatures up to 1400 K [1–3]. High fluence of neutron irradiation introduces various changes in physical properties of the materials, especially in thermal diffusivity. Thermal diffusivity is one of the most important factors for the plant efficiency.

Thermal conductivity K(W/K·m) is obtained as $K = \alpha C_p \rho$, where C_p (J/K·kg) is specific heat at constant pressure and ρ (kg/m^3) is density. Change in density after an irradiation is measured by linear or volume swelling, but the amount is not so large ($< 2\%$), and the specific heat keep almost same after an irradiation [4]. So a change in thermal diffusivity almost represents a change in thermal conductivity.

In ceramic materials, unlike metals, heat is mainly carried by phonon. Phonon transportation is obstructed by two factors. Even in unirradiated ceramics, phonons are scattered among each other, and this phonon-phonon scattering increases with measurement temperature arise. In addition, phonon is scattered by lattice defects. This phonon-lattice scattering is decided by grain size or concentration of impurity in the case of unirradiated ceramics, but neutron irradiated material contains many lattice defects, especially vacancy scatters phonon severely. Hence, it has also been reported that neutron-irradiated specimens show severe degradation in the thermal diffusivity [5–12].

These post irradiation measurements were performed at room temperature to specimens after the irradiation. Nevertheless, it is very important to estimate the thermal diffusivity during the irradiation. But it is very difficult to measure thermal diffusivity during neutron irradiation directly. So it is required to estimate that from the post irradiation measurement, with consideration of both phonon-phonon scattering and phonon-lattice scattering.

Thermal diffusivity α (m^2/s) of neutron-irradiated ceramics depend on measured temperature T(K) as $\alpha = k/T^n$, where k is the constant that is related to the absolute value, and n is the constant that represents the state of induced defects. The n constant is usually 1 for unirradiated ceramics, but it decreased with the irradiation, so it is not easy to

estimate the thermal diffusivity at elevated temperature from the measurement at room temperature [13; 14]. In addition, to estimate the thermal diffusivity during the irradiation from the post-irradiation measurement, it must be assumed that specimens after an irradiation would retain the same amount of defects as during the irradiation. It requires quick quench of the specimens after the irradiation and that defects are stable below the irradiation temperature. In addition, the specimen during an irradiation, interstitial atoms and vacancies are created by neutron and knock-on atoms. Most of them recombine in very short time, but in bulk specimen, several numbers of defects exist along with the stable defects. This defects that exist in very short time during an irradiation are called transient defects. Neutron irradiation flux and temperature may change the number of these transient defects. To estimate the thermal diffusivity during an irradiation from the post-irradiation measurements, amount of these transient defects must enough small. To confirm these assumption, many experiments were performed explained in three sections.

At first, degradation of thermal diffusivity with neutron irradiation dose was measured at room temperature [6; 8–10]. Around 30 dpa, the degradation was almost saturated with neutron dose, and that indicates thermal diffusivity would almost stable for very high-fluence applications.

And the next, annealing behavior showed that defects in post-irradiation specimens are stable under the irradiation temperature[5]. So, quenched defects in an irradiated specimen would keep the same amount during post-irradiation measurements operated under the irradiation temperature.

At last, transient defects are considered. Dynamic effect by transient defects during irradiation is an important issue to resolve the defect-production processes, but experimental study was very few [15–17]. Ion-beam irradiation is conventional method to investigate irradiation effects, but ion-beam induces defects in very shallow range near the surface, so the change in thermal diffusivity after an ion-beam irradiation may not be detectable. Nowadays, positron annihilation lifetime (PAL) has been measured to investigate the irradiation defects. This PAL is sensitive to distribution of vacancy-like defects, and thermal diffusivity in ceramics is also primarily controlled by the same defect. In addition, positron can probe local defects induced in small area by themselves, so defects induced by ion-beam irradiation expected to be observed with this method.

In this study, positron annihilation lifetime was measured on heavily neutron irradiated ceramics to clarify the correlation between PAL and thermal diffusivity. Several specimens showed significant change after the irradiation in PAL, but the difference in PAL and also thermal diffusivity were too small to estimate the correlation because the irradiation was to heavy and the amount of defects were almost saturated. So, electron irradiation was used to induce defect to lower dpa than the neutron irradiated specimens. From these measurements, the correlation between PAL and thermal diffusivity was suggested. And then, in-situ PAL measurements during ion-beam measurements were performed. The results were considered to deny the contribution of transient defects to thermal diffusivity.

Finally, thermal diffusivity of ceramics during the irradiation was estimated and showed almost flat profile with the irradiation temperature [13; 14].

2. Saturation in degradation of thermal diffusivity

In this section, degradation of thermal diffusivity measured at room temperature that depends on neutron irradiation dose and irradiation temperature is discussed.

ID	T51	T52	T53	T54	T55	T56	T57	T58	T71	T72	T73
neutron fluence (10^{26} n/m^2)	2.8	5.3	3.9	7.3	4.2	8.0	3.7	6.9	0.5	1.4	0.4
irradiation temperature (K)	775	775	864	835	1004	950	1011	1039	646	668	853

Table 1. Neutron irradiation conditions

Specimens were heavily neutron-irradiated in the experimental fast reactor JOYO using CMIR-4 rig, and several specimens (T52, T54, T56 and T58) were irradiated also in CMIR-5 rig. Four kinds of materials, α-Al_2O_3, AlN, β-Si_3N_4 and β-SiC were enclosed in the same capsule. Irradiation conditions for each specimen are listed in Table 1, and additional details for several specimen are listed in Table 2. The dimensions of the specimens were 3 mm diameter and 0.5 mm height for T5x specimens and 10 mm diameter and 2 mm height for T7x specimens.
Thermal diffusivity was measured by the laser flash method with the $t_{1/2}$ analysis [18] using a specially ordered ULVAC TC-7000 that can measure ϕ3 mm$\times$ 0.5 mm (T5x) specimens. The measurements were performed at room temperature. Specimens were coated by a carbon spray and baked on a hot plate at about 373 K before the measurement to reduce translucence of AlN and α-Al_2O_3 and to equalize the temperature on the surface of specimen.
Figs. 1a to 1d show the thermal diffusivity measured at room temperature for each material depend on neutron-irradiation dose. These results showed that β-Si_3N_4 specimens maintained the highest thermal diffusivity after neutron irradiation, compared to α-Al_2O_3, AlN and even β-SiC. In Figs. 1, number in parentheses under a specimen ID shows the irradiation temperature (K). Specimens were separated into two groups by irradiated temperature, and specimens irradiated at relatively high temperature (950-1039 K) are shown with open symbols, while solid symbols represent lower temperatures (646-864 K). With this grouping, the data shows that the dose dependence of thermal diffusivity saturated near 3×10^{26} n/m^2 for all materials here.
After the saturation with neutron dose, thermal diffusivity was simply determined by the irradiation temperature. That is, thermal diffusivity measured at room temperature after an irradiation increased slightly with the irradiation temperature rose.
Figs. 2a to 2d show the relationship of thermal diffusivity measured at room temperature after an irradiation and the irradiation temperature for each material. In this figure, a number in parentheses under a specimen ID gives the neutron fluence (10^{26}n/m^2). It is easy to see that T7x specimens with solid symbols showed higher thermal diffusivity than the other specimens irradiated more than 3×10^{26} n/m^2 presented with open symbols. This verifies that T7x specimens were not saturated with the neutron fluence, while T5x specimens irradiated more than 3×10^{26} n/m^2 reached saturation and the thermal diffusivity was determined only by the irradiation temperature.
In Figs. 1c and 1d, the T71 specimens showed relatively low thermal diffusivity at that neutron dose. T71 specimens were irradiated at 646 K and the microstructure of a β-Si_3N_4 specimen was observed by HREM [19]. It showed that the T71 β-Si_3N_4 specimen contained no obvious interstitial dislocation loops but poorly defined clusters or small rudiment of loops, while the T72 specimen irradiated at 668 K contained clear dislocation loops. In addition, the annealing behavior of swelling and thermal diffusivity in T71 β-Si_3N_4 specimens was obviously different from that in T72 or T73 specimens [8; 19]. The behavior showed that at 646 K interstitial atoms were not enough mobile to create interstitial dislocation loops or to annihilate with non-neighboring vacancies, therefore many isolated interstitial atoms and vacancies remain. This difference in microstructure of irradiation induced defects caused lower thermal diffusivity of T71 specimen than the other specimens. This also caused

material	α-Al_2O_3	AlN	β-Si_3N_4	β-SiC
manufacturer	Nippon Steel	Tokuyama	Nippon Steel	Nippon Steel
product name	NSAR	Super Shapal	NS101	SiC
raw material	α-Al_2O_3 100wt%	AlN (unknown)	β-$Si_3N_4 > 88$wt% $Y_2O_3 < 10$wt% $ZrSi_2 < 2$wt%	β-SiC > 99wt% $Al_2O_3 < 1$wt%
sintering method	pressureless	pressureless	hot-press	hot-press
thermal diffusivity ($10^{-4}\,m^2/s$)	0.118	0.991	0.250	0.410
dencity ($10^3\,kg/m^3$)	3.96	3.25	3.33	3.20
specific heat ($10^3\,J/kg{\cdot}K$)	0.789	0.738	0.636	0.697
thermal conductivity (W/m·K)	36.9	238	53.0	91.4

Table 2. Properties of specimens for neutron irradiation

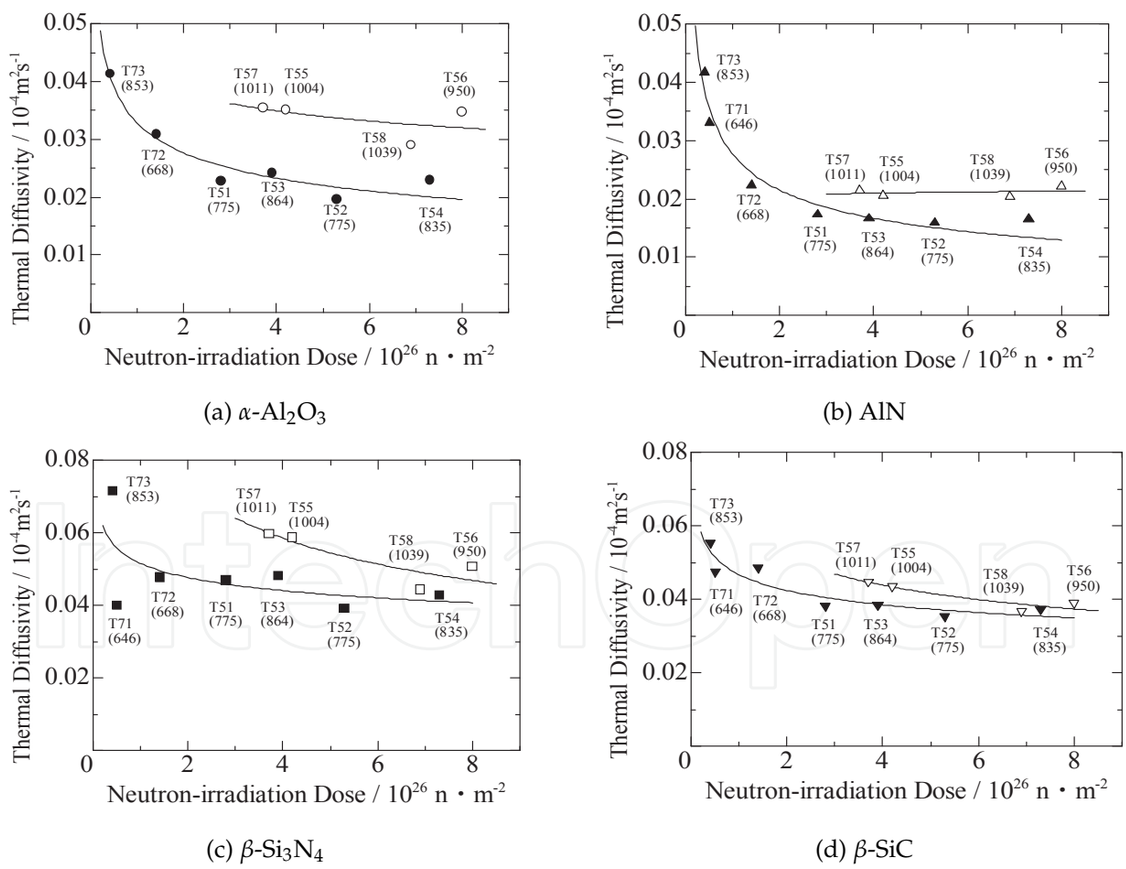

(a) α-Al_2O_3 (b) AlN

(c) β-Si_3N_4 (d) β-SiC

Fig. 1. The dose dependence of thermal diffusivity for each material. A number in parentheses under a specimen ID gives the irradiation temperature (K). Specimens they were irradiated at relatively high temperatures are shown by open symbols, and irradiated at lower temperatures shown by solid symbols.

significant difference in swelling behavior, and the T71 α-Al_2O_3 specimen was hardly cracked and thermal diffusivity could not be measured.

In ceramic materials, the thermal diffusivity is proportional to the mean free path of phonons. This mean free path can be heavily affected by irradiation induced defects, especially vacancies. The mean free path of phonons after irradiation (λ_I) is given as $1/\lambda_I = 1/\lambda_0 + 1/\lambda_d$ where λ_0 is for non-irradiated material and λ_d is related to the irradiation induced defect. Experimentally, λ_0 and λ_I were obtained from measured thermal diffusivity before and after irradiation, with the expression $\alpha = \frac{1}{3}\mu\lambda$ [4]. In this expression, μ (m/s) represent the mean speed of phonon, and it was calculated from $\mu = \sqrt{E/\rho}$ where E (Pa) is the Young's modulus and ρ (kg/m^3) is the density.

The λ_0, reflect the thermal diffusivity of non-irradiated specimen, is affected by many factors, such as grain shape, grain boundary structure, impurities or sintering agents. However, these effects are insignificant in irradiated materials, because dimensions of these defects are far large compared to that of irradiation defects.

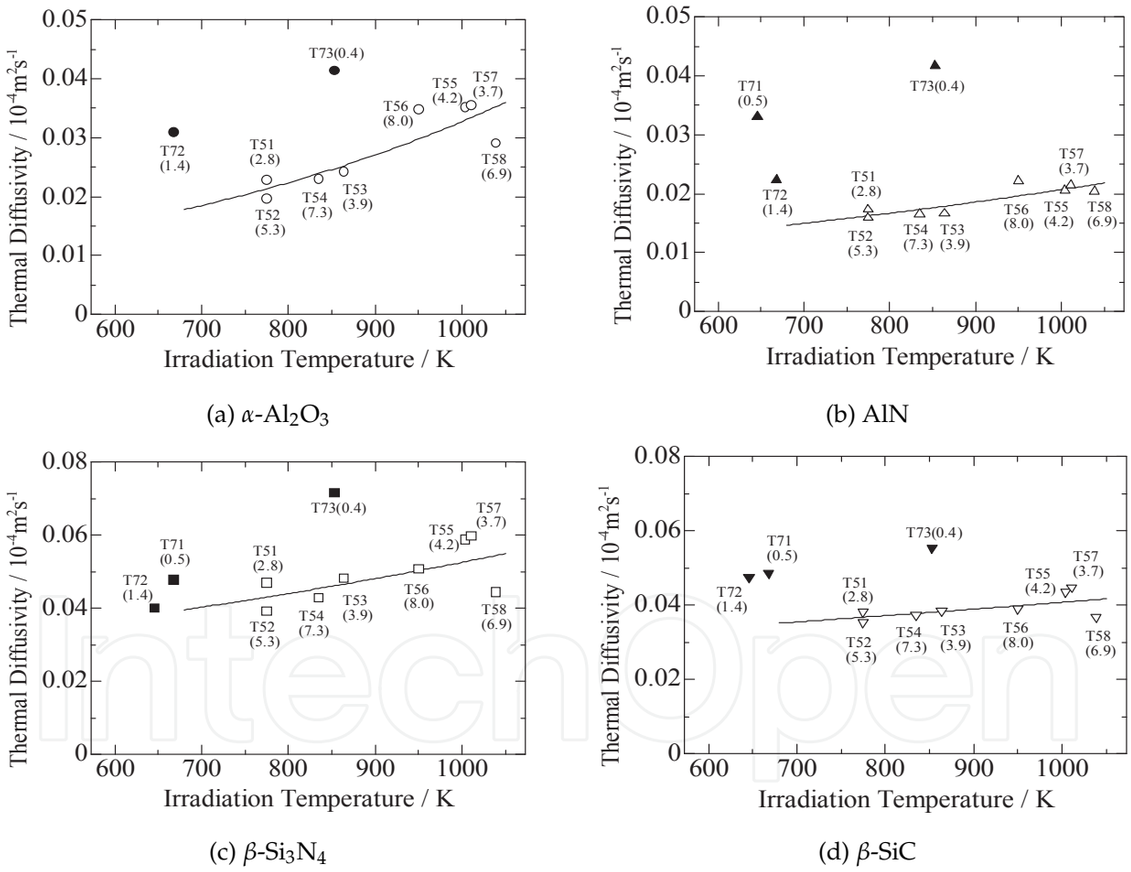

(a) α-Al_2O_3 (b) AlN

(c) β-Si_3N_4 (d) β-SiC

Fig. 2. Dependence of thermal diffusivity on irradiation temperature for each material. A number in parentheses under a specimen ID gives the neutron fluence (10^{26} n/m^2). Specimens they were irradiated to relatively high neutron fluences ($> 3 \times 10^{26}$ n/m^2) are shown with open symbols, and to lower fluences shown with solid symbols.

3. Annealing behavior after the irradiation

In this section, annealing behavior was studied to make sure that defects in irradiated specimen keeps the same amount during post-irradiation measurements operated under the irradiation temperature.

The neutron-irradiation conditions for ceramic specimens are the same in the previous section (Table 1). Thermal diffusivity was measured by the same method in the previous section, too. Isochronal annealing was conducted every 100 K up to 1773 K in a vacuum of $<$ 1 Pa ($<$1273 K) or $<$ 10^{-4} Pa (1373 - 1773 K). Specimens were annealed for 1 h at an objective temperature. After the annealing, specimens were cooled in the furnace, and each measurement was performed at room temperature.

Figs. 3a to 3h show recovery behavior of thermal diffusivity by isochronal annealing in neutron-irradiated ceramics. From the limitation of space, irradiation condition of T51 (2.8×10^{26} n/m^2, 775 K) and T57 (3.7×10^{26} n/m^2, 1011 K) are mentioned here.

Figs. 3a and 3b show recovery behavior in α-Al_2O_3. The recovery started around the irradiation temperature along with parabolic curves, and then it changed to linearly around 1423 K. This moderation at high temperature may cause saturation of recovery. After the annealing of 1773 K, the thermal diffusivity was recovered to about 80% of non-irradiated Al_2O_3. From the microstructure observation of neutron-irradiated α-Al_2O_3 with TEM, both interstitial atom and vacancy have enough mobility to make interstitial dislocation loops or voids at least above 775 K while the recovery started above 1073 K in T57. The temperature on which the recovery started rose with the irradiation temperature, and in Fig. 3a recovery started around 973 K. It is thought that activation energy to recombine of interstitial loops and vacancies changes with size of loops, and the size changed with the irradiation temperature. The linear recovery at higher temperature is usually solved with sintering-like process that dissolve voids and micro cracks.

Figs. 3c and 3d show recovery behavior in AlN. In both Fig. 3c and Fig. 3d, the recovery of thermal diffusivity started around 1173 K. Above the temperature, mobility of vacancy is seemed to be enough to annihilate with interstitial loops. Unlike α-Al_2O_3 formed by ionic bond, AlN, β-Si_3N_4 and β-SiC are formed by covalent bond, and vacancies are not mobile at relatively low temperature (below 1173 K) while interstitial atoms enough mobile to gather interstitial dislocation loops around 573 K.

Figs. 3e and 3f show recovery behavior in β-Si_3N_4. In the β-Si_3N_4 that was irradiated to high dose, nano-partition structure was formed [20], and it restricted growth of loops, so interstitial atoms lost sink and recombined with vacancies. The fast recovery above 1273 K is interpreted that vacancies were enough mobile above 1273 K to recombine with small loops. But obvious length or density change of loops and also formation of voids were not observed by TEM in specimens annealed to 1773 K. In Fig. 3f thermal diffusivity was recovered a little around 773 K, that was lower than the irradiation temperature. This problem was discussed with β-SiC described below. All specimens in this study showed recovery from the same temperature of 673 - 773 K, and it was considered to be the threshold where interstitial atoms get mobile and recombine with vacancies.

Figs. 3g and 3h show recovery behavior in β-SiC. It is well known that β-SiC showed linear recovery in swelling from an irradiation temperature, and with annealing to 1773 K, swelling was recovered completely [21; 22]. Several interstitial atoms on the edge of dislocation loops separate from the edge and growth to larger loops or recombine with vacancies. A stability of an interstitial dislocation loop is decided by the size of the loop, and a distribution of the size was determined by irradiation temperature. It may cause the recovery from the

irradiation temperature. However, Fig. 3h shows a recovery in thermal diffusivity started below the irradiation temperature. Most possible reason is that the sample was irradiated lower temperature than the nominal irradiation temperature while the reactor was shutting down and suffered remarkable effect. It was reported that the JOYO fast reactor have high neutron flux of 5×10^{19} n/m^2·s near the core that gives about 2×10^{24} n/m^2 (0.2 dpa) within 12 h. This neutron flux might get smaller during the shut down the reactor, but even neutron flux of 1×10^{23} n/m^2 (0.01 dpa) gives enough degradation in thermal diffusivity examined with electron irradiation described in the next section. All β-SiC specimens in this study showed recovery from 673 - 773 K, and it was explained that interstitial atoms get mobile and recombine with vacancies, same as in β-Si_3N_4. Further more, Fig. 3h shows change of trend around the nominal irradiation temperature, which signifies the sample was surely irradiated at the temperature for most of the irradiation term.
It is concluded that the number of vacancies induced by neutron irradiation keeps almost same amount below the irradiation temperature. α-Al_2O_3 and AlN showed no recovery below 973 K even irradiated lower temperature. It can be said in other word, the temperature where recovery of thermal diffusivity start did not depend on the irradiation temperature. β-Si_3N_4 and β-SiC showed a little recovery below the irradiation temperature, but it may arose from the shutting down process of the irradiation, and at least, defects were not recovered below 673 K.

4. Estimation an amount of transient defects during irradiation

In this section, amount of transient defects during irradiation was estimated from positron annihilation lifetime.
Nowadays, positron annihilation lifetime (PAL) has been widely used for many material studies to investigate the distribution of defects. Both PAL and thermal diffusivity are sensitive to distribution of vacancy-like defects, but the correlation was not clarified.
In this section, at first, PAL in neutron irradiated specimen was measured to clarify the correlation with thermal diffusivity. Several specimens showed significant change on PAL after the neutron irradiation, but the difference in PAL and also thermal diffusivity between irradiated specimens was too small to estimate the correlation, because the irradiation was too heavy and the amount of defects were almost saturated. So next, high-energy electron irradiation was performed to induce defect to lower dpa than the neutron irradiated specimens. From these measurements, the correlation between PAL and thermal diffusivity was suggested.
After that, in-situ PAL measurement during ion-beam irradiation was challenged to estimate the amount of transient defects during irradiation.

4.1 Correlation between positron annihilation lifetime and thermal diffusivity

Electron irradiations were performed using 30 MeV electron linac in Kyoto University Research Reactor Institute. The beam current was 110 - 170 μA in 2 cm^2 in average. The range of 30 MeV electron was about 5 cm in ceramics, and the defects were induced equally allover the $\phi 3 \times 0.5$ mm specimens. The specimens were irradiated at 300 - 310 K in cooling water and the electron irradiation dose was $1.3 - 3.0 \times 10^{24}$ e/m^2 that correspond to $0.93 - 2.1 \times 10^{-2}$ dpa. Detail of irradiation conditions were listed in Table 3.
The specimens prepared for the electron irradiations were different from the neutron irradiations. The specimens for neutron-irradiation were quite unique products looking for liquid-metal cooling fast reactor. But the number of non-irradiated specimens was limited

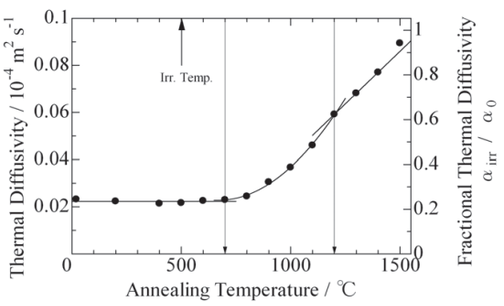

(a) α-Al_2O_3 T51 (2.8×10^{26} n/m^2, 775 K)

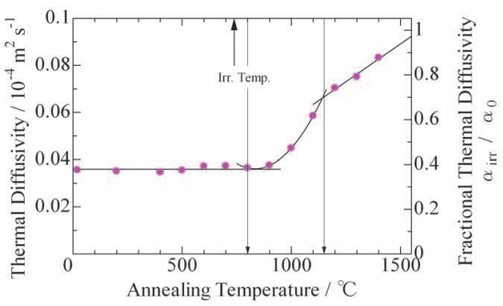

(b) α-Al_2O_3 T57 (3.7×10^{26} n/m^2, 1011 K)

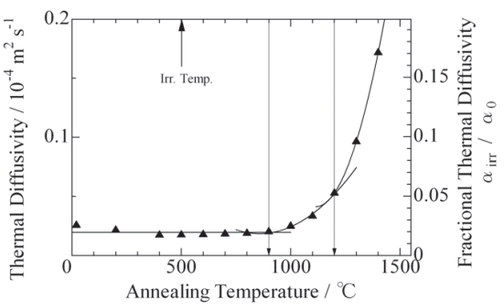

(c) AlN T51 (2.8×10^{26} n/m^2, 775 K)

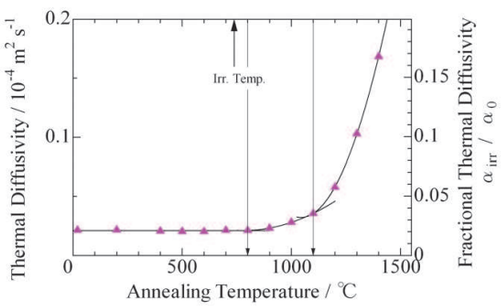

(d) AlN T57 (3.7×10^{26} n/m^2, 1011 K)

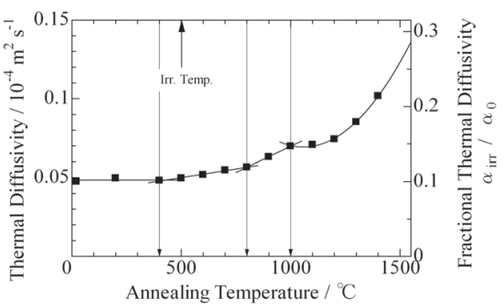

(e) β-Si_3N_4 T51 (2.8×10^{26} n/m^2, 775 K)

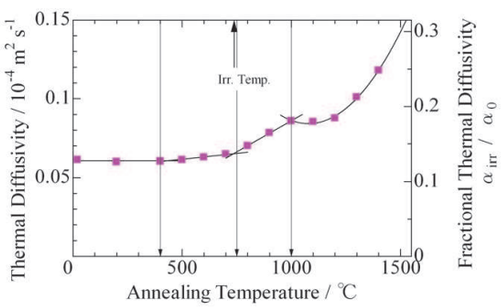

(f) β-Si_3N_4 T57 (3.7×10^{26} n/m^2, 1011 K)

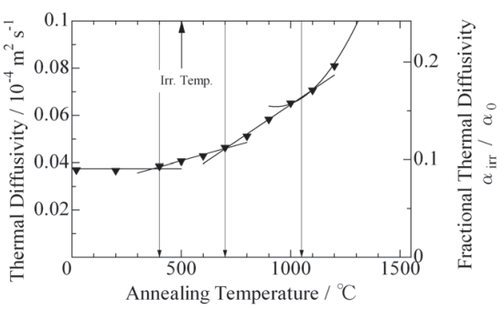

(g) β-SiC T51 (2.8×10^{26} n/m^2, 775 K)

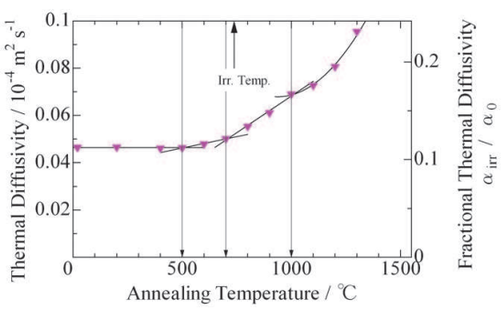

(h) β-SiC T57 (3.7×10^{26} n/m^2, 1011 K)

Fig. 3. Recovery behavior of thermal diffusivity by isochronal annealing in neutron-irradiated ceramics

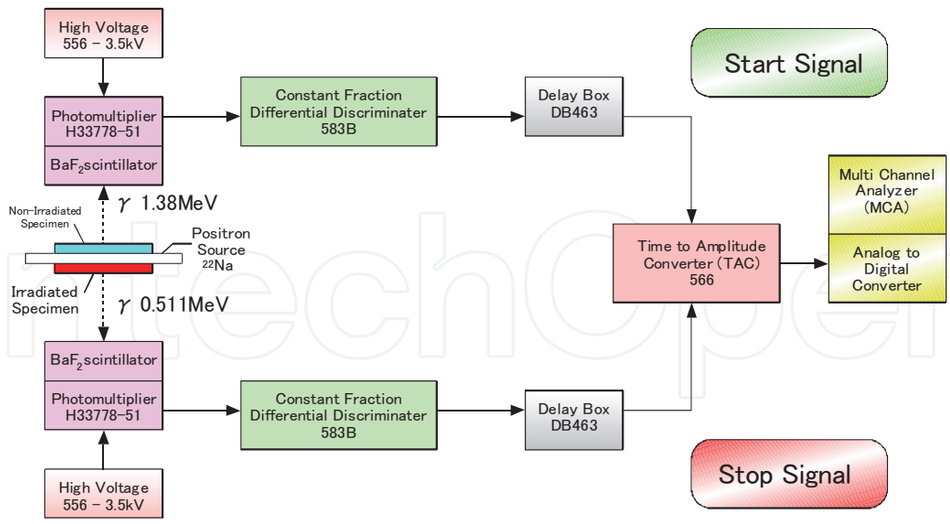

Fig. 4. Conventional γ-γ coincidence circuit-diagram to measure PAL in specimen after an irradiation

and the detail was not publicized, so in this study, specimens for electron irradiation were supplied from the market. Properties of these specimens were listed in Table 4.
Positron annihilation lifetime was measured by conventional $\gamma - \gamma$ fast coincidence method, and the circuit-diagram is shown in fig. 4. Our facility allows only sealed ^{22}Na source, and the diameter of irradiated specimens were only 3 mm. So, the PAL measurements were performed with specially ordered ^{22}Na 1 MBq positron source that have active diameter of 1 mm sealed by 12.7 μm Ti foil. The positron from ^{22}Na have an energy 0.55 MeV in maximum that reaches 0.5 mm in ceramics, but the average range was 100μm. The measurements were performed at room temperature.
In addition, a positron source is put between two specimens at ordinary setup. However, only one disk was prepared for each irradiation condition in this study, so a non-irradiated

ID	KURL0708	KURL0801	KURL0802
electron fluence [e/m^2]	1.5×10^{24}	1.3×10^{24}	3.0×10^{24}
irradiation dose [dpa]	1.0×10^{-2}	0.93×10^{-2}	2.1×10^{-2}
irradiation temperature [K]	300	310	310

Table 3. Electron irradiation conditions

material	α-Al_2O_3	AlN	β-Si_3N_4	β-SiC
manufacturer	Toray	Tokuyama	Toray	Bridgestone
product name	A-999	SH-30	SN	PB-S
sintering method	pressureless	pressureless	hot-press	hot-press
thermal diffusivity [10^{-4} m^2/s]	0.122	0.744	0.110	1.07
dencity [10^3 kg/m^3]	3.9	3.34	3.2	3.15
thermal conductivity [W/m·K]	38	174	25	230
volume resistivity [Ω·cm]	$> 10^{14}$	8.4×10^{13}	$> 10^{14}$	2.0×10^{-2}

Table 4. Properties of specimens for electron irradiation

specimen was located at the other side of an irradiated specimen. This treatment may change intensity of long lifetime component, but not change bulk and long lifetime itself.
The obtained PAL spectrum was analyzed with PALSfit program [23], with resolution FWHM about 300 ps at first and improved gradually to 230 ps at last. The analyzed positron lifetimes are described as τ_1: short lifetime and τ_2: long lifetime, and I_i are the intensities for each components. The average positron lifetime $\langle\tau\rangle$ is obtained as $\langle\tau\rangle = \tau_1 I_1 + \tau_2 I_2$. In this study, source component that represent annihilation of positron in Ti foil was not resolved since the PAL of Ti was measured as τ_1: 136 ps (97 %), τ_2: 447 ps (3 %) and $\langle\tau\rangle$: 145 ps that is very close to the PAL in ceramics. So only two components were guessed in the analysis.
Electron irradiated ceramics to doses of 0.01 - 0.02 dpa showed distinct changes in thermal diffusivity. α-Al_2O_3 and β-Si_3N_4 showed rather low thermal diffusivity before the irradiation (about 0.11×10^{-4} m^2/s), and it showed small degradation to 0.08×10^{-4} m^2/s. On the other hand, thermal diffusivity of non-irradiated AlN and β-SiC were 0.73 and 0.95 $\times 10^{-4}$ m^2/s, and they decreased to 0.46 - 0.65 and 0.23 - 0.40 $\times 10^{-4}$ m^2/s for each.
PAL measurements were performed on neutron irradiated specimens at first, and then on electron irradiated specimens mentioned above. The correlation between thermal diffusivity and PAL is presented in Fig. 5.
Neutron and also electron irradiated α-Al_2O_3 showed obvious increment in $\langle\tau\rangle$ with degradation of thermal diffusivity as shown in Fig. 5a. In this study, electron irradiated α-Al_2O_3 showed relatively small change in thermal diffusivity, but large change in PAL at the dose of 0.01-0.02 dpa. It is said that PAL detect vacancy-like defects in crystal more sensitive than thermal diffusivity at early stage of irradiation.
AlN in Fig. 5b showed almost the same feature in Al_2O_3. This result shows $\langle\tau\rangle$ was saturated in early stage of irradiation, too. Heavily neutron irradiated AlN showed almost same thermal diffusivity and PAL, but electron irradiated AlN showed correlation between thermal diffusivity and PAL. Kanechika et al. reported similar correlation even in non-irradiated specimens sintered in different conditions [24].
However in Fig. 5c, β-Si_3N_4 specimens showed no increment or rather decrement in $\langle\tau\rangle$ with degradation of thermal diffusivity. In addition, average lifetime of non-irradiated β-Si_3N_4 prepared for neutron irradiation was 216$\pm$8 ps and for electron irradiation was 226$\pm$2 ps, which is larger than any other ceramics in this work (about 150 ps). This result is considered to arise from large barrel structure surrounded by six SiN_4 tetrahedron that penetrate the crystal perpendicular to the (0001) plane. Neutron irradiated β-Si_3N_4 contained larger 'peanuts' like structures [25; 26], but the fraction in the crystal was small. It is considered that most positron annihilated in this large empty structure and showed long lifetime, so small number of vacancies did not affect the PAL in irradiated β-Si_3N_4.
β-SiC showed also almost no change after the neutron irradiation in Fig. 5d, but the electron irradiated specimens prepared from 'pure-β' SiC (Bridgestone) showed a little increment. However, many works reported change of PAL in SiC irradiated by electron or ion beam [27–33]. Kawasuso et al. reported that electron irradiated n-type (nitrogen-doped) 6H-SiC showed obvious change in $\langle\tau\rangle$ (143 ps to 178 ps), while p-type (aluminum-doped) 6H-SiC showed almost no change (136 ps to 138 ps) [33]. The specimen was irradiated with 3 MeV electron to a fluence of 1×10^{17} e$^-$/cm^2, that correspond to about 4×10^{-6} dpa. And also Henry et al. reported 6H-SiC that was irradiated by 12 MeV proton up to 4×10^{15} showed same tendency [29]. In this work, β-SiC specimens used for neutron irradiation were sintered with 1% Al_2O_3, so it was possible that the crystal contains several aluminum that makes the specimens p-type. On the other hand, β-SiC specimens for electron irradiation were sintered

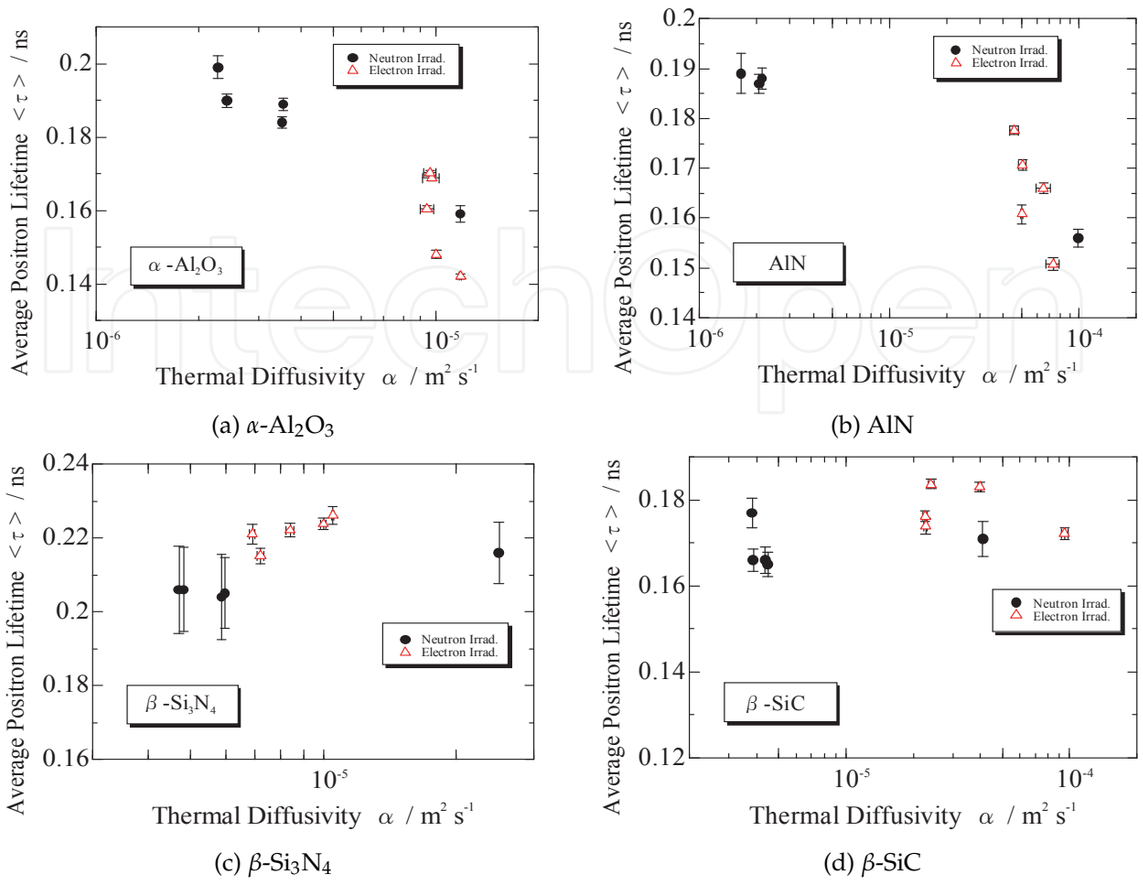

(a) α-Al_2O_3 (b) AlN

(c) β-Si_3N_4 (d) β-SiC

Fig. 5. Change of average positron lifitime $\langle\tau\rangle$ in neutron irradiated ceramics compared with thermal diffusivity

without any sintering additive, and electron irradiated specimen showed a little increment in PAL, but the change was very small and the relation between thermal diffusivity and the PAL was not sure.

From these result, 30 MeV electron irradiation and PAL measurement is good combination to investigate the distribution of defects in several materials. Using KURRI-Linac, irradiation at elevated temperature (up to 1400 K) is available, and it may give many contributions to clarify the behavior of defect. Anyway, thermal diffusivity has some correlation with positron annihilation lifetime, at least α-Al_2O_3 and AlN.

4.2 In-situ PAL measurement during ion-beam irradiation

It was concluded that α-Al_2O_3 and AlN showed some correlation between thermal diffusivity and PAL measured after the irradiation. And then, in-situ PAL measurement during ion-beam irradiation is examined to clarify the amount of transient defects is enough small.

To execute in-situ measurement during ion-beam irradiation, conventional $\gamma - \gamma$ coincidence system (Fig. 4) can not be applied, because this system requires symmetrical specimen and detector arrangement to create start and stop signal, and they obstructs ion-beam irradiation. In this study, asymmetric $\beta - \gamma$ coincidence system was applied using avalanche photodiode (APD) for a device to detect a positron and give a start pulse (Fig. 6). Usually APD is used to detect photon and the crystal is rather thick, but in this system positron penetrates the crystal

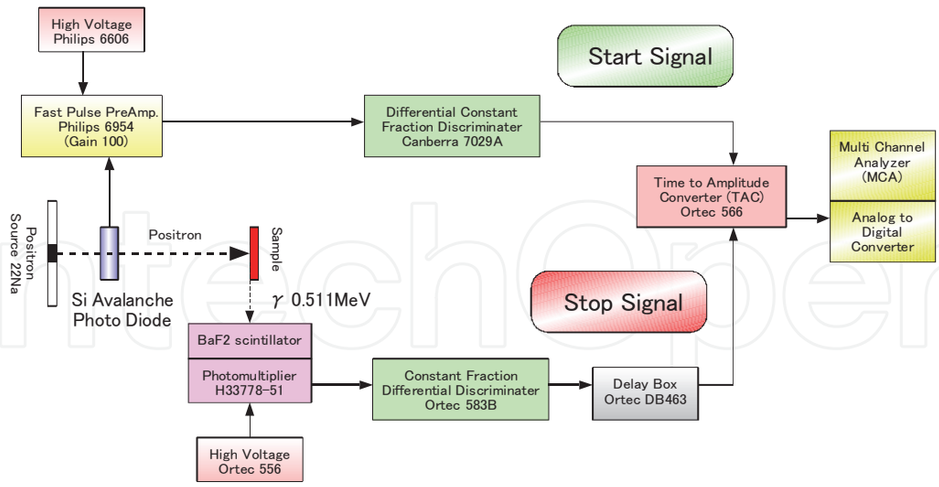

Fig. 6. Circuti-diagram using β-γ coincidence for in-situ PAL measurement during ion-beam irradiation

to reach a specimen, so the thickness of Si in the APD was 110 μm in the size of $5\times5\,\mathrm{mm}^2$ (EG & G Optoelectronics, C30626-CD2274). The pulse height from APD is fixed by energy of incident positron, and that enables to select the depth where the positron was injected and annihilate. Ion-beam irradiation induces defects within very shallow range, so the pulse from APD is selected by Constant Fraction Differential Discriminator (CFDD) to match the defect induced area and positron annihilation area. Positron source in this measurement was ^{68}Ge that irradiate almost no γ-ray when a positron is projected unlike ^{22}Na. The positron source was arranged crossly at the same side of the specimen irradiated by ion-beam.

At first, PAL in a specimen before irradiation was measured at room temperature. Then the specimen was irradiated by ion-beam and in-situ PAL measurement was performed during the irradiation. Ion-beam irradiation was conducted by 2.0 MeV H^+ with a flux of $1.2\times10^{16}\,\mathrm{ion/m^2\cdot s}$ using a Van de Graaff accelerator in Radiation Laboratory, Uji, Kyoto University. The irradiation and measurement was operated for 6×10^4 sec, to a fluence of $7\times10^{20}\,\mathrm{ion/m^2}$ that corresponds to 5.8×10^{-2} dpa. After the irradiation, PAL was measured again.

The obtained in-situ PAL spectrums are shown in Figs. 7a to 7d. In Fig. 7a, spectrum illustrated by solid dot represents the specimen before the irradiation, and the spectrum after and during the irradaition showed larger intensity around 1 - 1.5 ns. This difference represents that this measurement can detect the static defects remain after the irradiation. On the other hand, because of the limitation of resolution and S/N ratio, certain lifetime was not analyzed, but it is said that difference between after and during the irradiation was not larger than the difference between before and after the irradiation of 5.8×10^{-2} dpa. AlN showed almost same tendency in Fig. 7b.

Fig. 7c and 7d shows the in-situ PAL spectrum in β-Si_3N_4 and β-SiC, respectively. Difference between the spectrum before, during and after the irradiation was not detected, and also β-Si_3N_4 showed same tendency. Just as the case of neutron-irradiated specimen, these spectrums showed that even static defects were not detected by positron annihilation measurement. Anyway, to evaluate the transient defects, more fine examination is expected in future work.

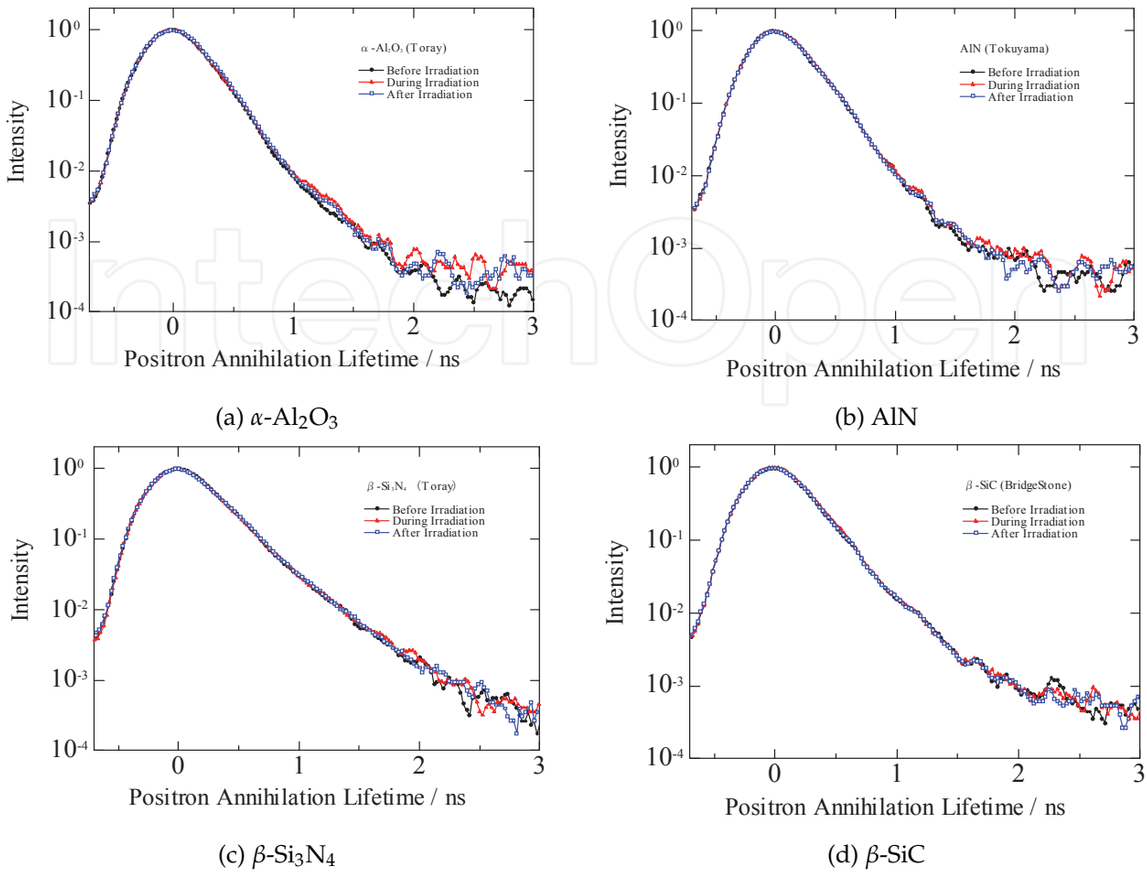

(a) α-Al_2O_3 (b) AlN

(c) β-Si_3N_4 (d) β-SiC

Fig. 7. PAL spectrum change among before, during and after ion-beam irradiation. Ion-beam irradiation was performed by 2.0 MeV H^+ with a flux of 1.2×10^{16} ion/m^2·s.

In addition, defect induced rate was discussed to evaluate the transient defect. In the specimen during irradiation, the interstitial atoms and vacancies are created by neutron irradiation, and subsequently, most of them recombine in a very short time. Neutron irradiation flux changes the amount of transient defects before recombination. In this study, the neutron irradiation dose of specimens irradiated in CMIR-4 rig reached 42 dpa (T55), that is said in other word, each atom was displaced 42 times during 176 days, and is calculated as 2.8×10^{-6} dpa/s. It indicates that the ratio of the transient defects that scatters phonon between the static defects is very small. During the in-situ PAL measurement above, the displacement ratio was calculated as 9.2×10^{-7} dpa/s. This rate is a little smaller than the ratio in the fast reactor JOYO, but enough larger than the ratio in Japan Material Testing Reactor, JMTR, 9.2×10^{-7} dpa/s. Dynamic effect by transient defects during irradiation is an important issue to resolve the defect-production processes [34], but the amount of transient defects is supposed too small to produce significant effect on thermal diffusivity.

5. Estimation of thermal diffusivity at the neutron irradiation temperature

In this section, thermal diffusivity during the irradiation was estimated from the post irradiation measurements. Thermal diffusivity α (m^2/s) of neutron-irradiated ceramics depend on measured temperature T (K) as $\alpha = k/T^n$. We assumed three assumptions, that is

1) Degradation of thermal diffusivity with irradiation is almost saturated above 30 dpa
2) Defects are stable until annealed above the irradiation temperature
3) Post-irradiated specimens kept the same amount of defects as during the irradiation.
Each assumption was confirmed in sections above. Then, thermal diffusivity at the irradiation temperature represents the thermal diffusivity during the irradiation. The n parameter in the equation $\alpha = k/T^n$ is 1 for non-irradiated ceramics, but after the irradiation, this n parameter decreased, so it is not easy to estimate the thermal diffusivity at elevated temperature from the measurement at room temperature.
In this section, thermal diffusivity was measured by the laser-flash method using specially ordered measurement system that can measure ϕ3 mm disk at high (up to 1723 K) and low (100-473 K) temperature (ULVAC-RIKO Inc. TC-7000H/L Special), and was analyzed with the t1/2 method. All the specimens were coated by graphite spray and baked on a hot plate at about 373 K to avoid transmission of laser flash. Measurements at elevated temperatures were performed for T52, T54, and T58 specimens using SiC furnace of TC-7000H system from room temperature to 1073 K, and a rapid increment of temperature after a laser flash was measured by IR sensor. After the measurement at 1073 K, all specimens showed recovery in thermal diffusivity at room temperature. Heavily-neutron irradiated specimen is very precious, and to avoid annealing effect even to the specimen irradiated relatively low temperature, measurements at low temperature were performed. After a laser flash, a rapid increment of temperature on the other surface of a specimen was measured by ϕ0.05 mm K-type thermocouple, because an intensity of IR from the cold surface is too small to measure with IR sensor. Thermocouple was attached on a surface of specimen using electroconductive epoxy (Circuit works CW2400) below 373 K to avoid annealing. Measurements at low temperature were carried out in He atmosphere ($< 10^4$ Pa), and a cryostat was cooled by liquid nitrogen. Measurements were taken at every 20 K from 123 K to 413 K.
Figs. 8 show thermal diffusivity of neutron-irradiated ceramics measured at room temperature to 1073 K. Open symbols at 1073 K represent as-measured values that contain annealing recovery. So, the thermal diffusivity at 1073 K plotted with solid symbols was modified via $\alpha_{1073} \times \alpha_0/\alpha_{an}$ where α_{1073} is the thermal diffusivity measured at 1073 K (plotted with open symbols), α_0 is measured at room temperature before annealing and α_{an} is measure at room temperature again after annealing to 1073 K. In addition, Figs. 9 show thermal diffusivity of neutron-irradiated ceramics measured at 123-413 K. From these measurements, n parameter was obtained. And then the thermal diffusivity at irradiation temperature, α_{irr}, was estimated as $\alpha_{irr} = \alpha_{300}(300/T_{irr})^n$ where T_{irr} represent the irradiation temperature and α_{300} the thermal diffusivity at 300 K measured by infrared sensor.
Finally, Figs. 10 show the estimated thermal diffusivity during the irradiation, α_{irr}, plotted with the irradiation temperature T_{irr}. For each material, α_{irr} was distributed in same line except T7x specimens. The T7x specimens were irradiated to 0.4-1.4 $\times 10^{26}$ n/m^2 and the degradation of thermal diffusivity was not saturated with neutron dose, on the other hand, the T5x specimens were irradiated to 2.8-8 $\times 10^{26}$ n/m^2 and saturated. It is expected that specimens irradiated more than 3×10^{26} n/m^2 at the irradiated temperature of T7x, α_{irr} may be distributed in the same line.
Estimated thermal diffusivities during the irradiation were almost independent on the irradiation temperature within the range of 775-1039 K, i.e., 1.5, 1.3, 2.7, 2.3$\times 10^{-6}$ m^2/s for α-Al_2O_3 , AlN, β-Si_3N_4 and β-SiC, respectively. β-Si_3N_4 kept highest thermal diffusivity during irradiation rather than the SiC. But in range of lower and higher irradiation temperature, behavior of defects basically different, and this flat profile may be changed at that range.

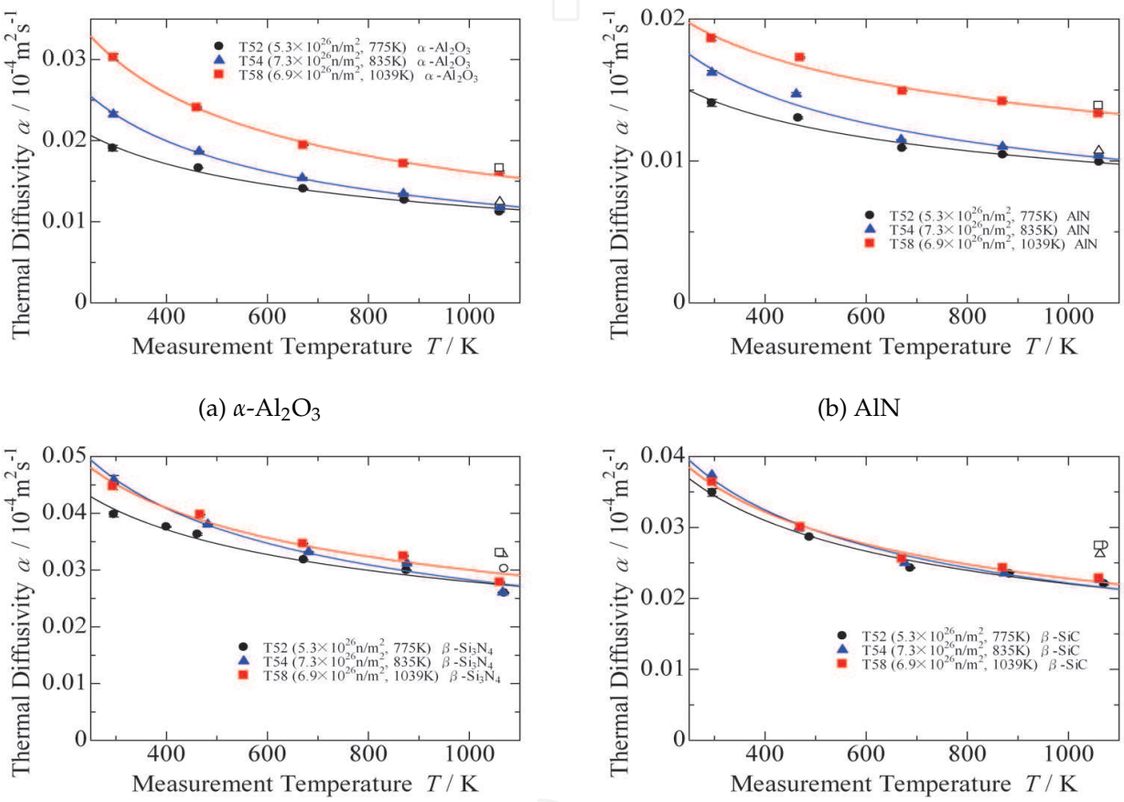

(a) α-Al_2O_3 (b) AlN

(c) β-Si_3N_4 (d) β-SiC

Fig. 8. Thermal diffusivity of neutron-irradiated ceramics measured at room temperature to 1073 K. Open symbols at 1073 K represent as measured values that contain annealing recovery, and the corrected values were plotted with solid symbols.

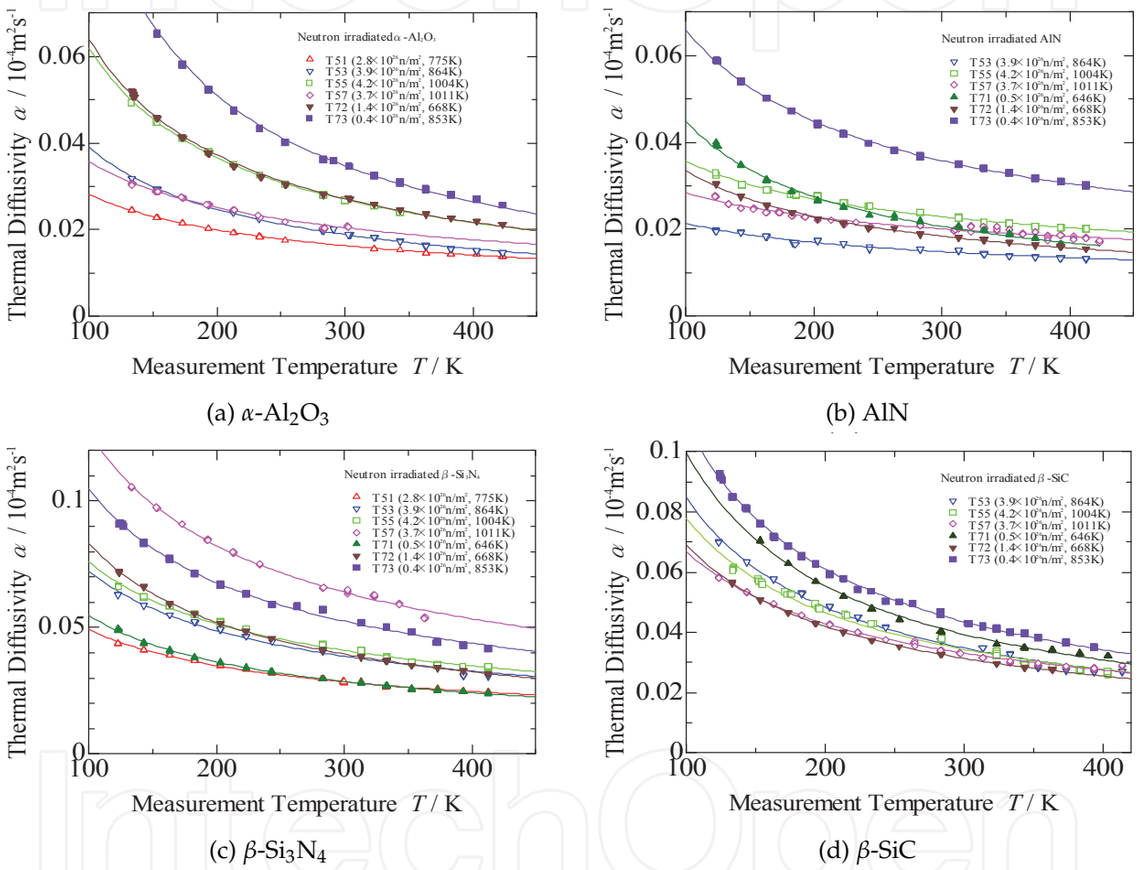

Fig. 9. Thermal diffusivity of neutron-irradiated ceramics measured at 123-413 K.

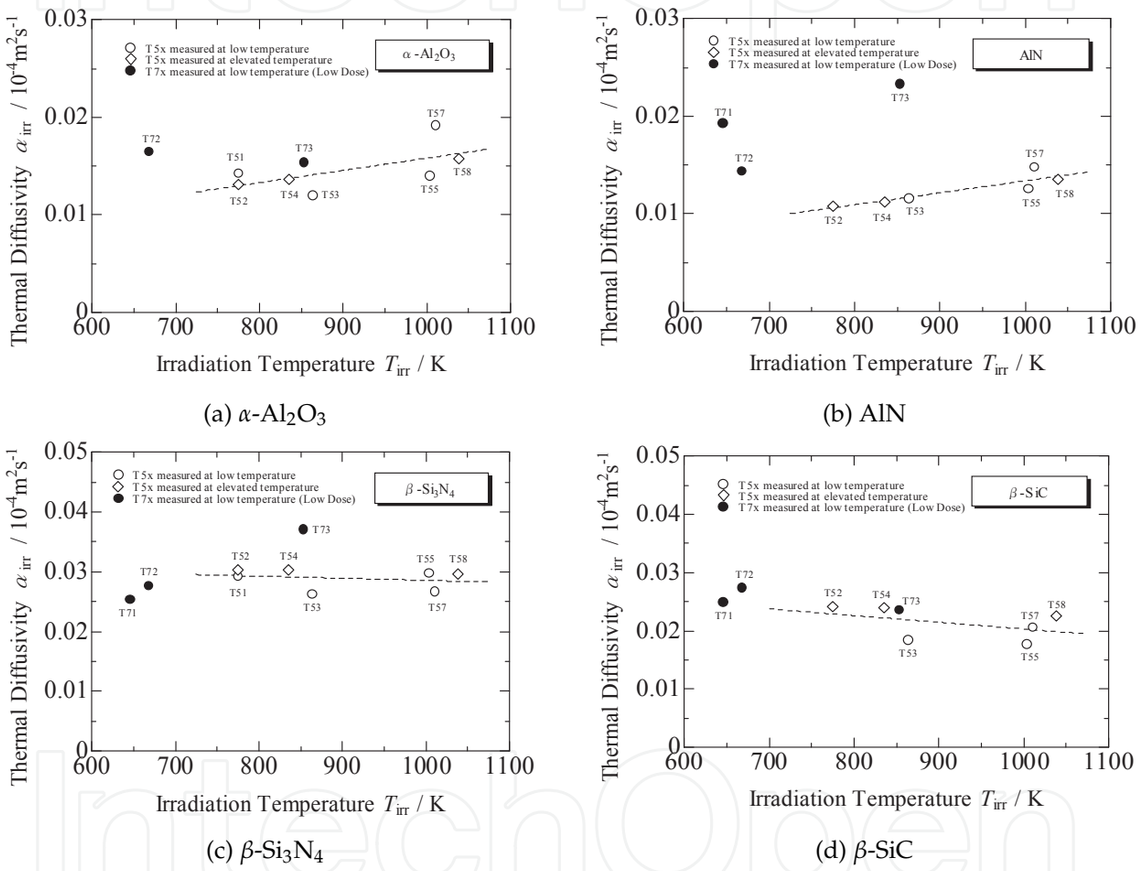

(a) α-Al_2O_3 (b) AlN

(c) β-Si_3N_4 (d) β-SiC

Fig. 10. Estimated thermal diffusivity of neutron-irradiated ceramics during the irradiation.

6. References

[1] Y. Katoh, L.L. Snead, C.H. Henager Jr., A. Hasegawa, A. Kohyama, B. Riccardi, and H. Hegeman. Current status and critical issues for development of SiC composites for fusion applications. *Journal of Nuclear Materials*, Vol. 367-370, pp. 659–671, 2007.

[2] T. Hino, E. Hayashishita, T. Yamada, X. Liu, A. Kohyama, Y. Yamauchi, Y. Hirohata, and Y. Nobuta. Progress of plasma surface interaction study on low activation materials. *Fusion Engineering and Design*, Vol. 81, pp. 181–186, 2 2006.

[3] R. Andreani, E. Diegele, R. Laesser, and B. van der Schaaf. The European integrated materials and technology programme in fusion. *Journal of Nuclear Materials*, Vol. 329-333, pp. 20–30, 2004.

[4] J.C. Corelli, J. Hoole, J. Lazzaro, and C.W. Lee. Mechanical, thermal, and microstructural properties of neutron-irradiated SiC. *Journal of the American Ceramic Society*, Vol. 66, No. 7, pp. 529–538, July 1983.

[5] M. Akiyoshi and T. Yano. Neutron-Irradiation Effect in Ceramics Evaluated from Macroscopic Property Changes in As-irradiated and Annealed Specimens. *Progress in Nuclear Energy*, Vol. 50, pp. 567–574, 2008.

[6] M. Akiyoshi, T. Yano, Y. Tachi, and H. Nakano. Saturation in degradation of thermal diffusivity of neutron-irradiated ceramics at $3\times10^{26}\mathrm{n/m^2}$. *Journal of Nuclear Materials*, Vol. 367-370, pp. 1023–1027, 2007.

[7] L. L. Snead, T. Nozawa, Y. Katoh, T. Byun, S. Kondo, and D. A. Petti. Handbook of SiC properties for fuel performance modeling. *Journal of Nuclear Materials*, Vol. 371, pp. 329–377, 2007.

[8] M. Akiyoshi, K. Ichikawa, T. Donomae, and T. Yano. Macroscopic properties and microstructure changes of heavily neutron-irradiated β-Si_3N_4 by annealing. *Journal of Nuclear Materials*, Vol. 307-311, pp. 1305–1309, 2002.

[9] T. Yano, M. Akiyoshi, K. Ichikawa, Y. Tachi, and Y. Iseki. Physical property change of heavily-neutron-irradiated Si_3N_4 and SiC by thermal annealing. *Journal of Nuclear Materials*, Vol. 289, pp. 102–109, 2001.

[10] T. Yano, K. Ichikawa, M. Akiyoshi, and Y. Tachi. Neutron irradiation damage in aluminum oxide and nitride ceramics up to a fluence of $4.2\times10^{26}\mathrm{n/m^2}$. *Journal of Nuclear Materials*, Vol. 283-287, pp. 947–951, 2000.

[11] C. Hazelton, J. Rice, L.L. Snead, and S.J. Zinkle. Effect of neutron radiation on the dielectric, mechanical and thermal properties of ceramics for rf transmission windows. *Journal of Nuclear Materials*, Vol. 253, pp. 190–195, 1998.

[12] M. Rohde and B. Schulz. The effect of the exposure to different irradiation sources on the thermal conductivity of Al_2O_3. *Journal of Nuclear Materials*, Vol. 173, pp. 289–293, 1990.

[13] M. Akiyoshi. Thermal diffusivity of ceramics at the neutron irradiation temperature estimated from post-irradiation measurements at 123-413 K. *Journal of Nuclear Materials*, Vol. 386-388, pp. 303–306, 2009.

[14] M. Akiyoshi, I. Takagi, T. Yano, N. Akasaka, and Y. Tachi. Thermal conductivity of ceramics during irradiation. *Fusion Engineering Design*, Vol. 81, pp. 321–325, 2006.

[15] K. Abe, A. Kohyama, C. Namba, F. W. Wiffen, and R. H. Jones. Neutron irradiation experiments for fusion reactor materials through JUPITER program. *Journal of Nuclear Materials*, Vol. 258-263, No. Part2, pp. 2075–2078, 1998.

[16] L.L. Snead, R. Yamada, K. Noda, Y. Katoh, S.J. Zinkle, W.S. Eatherly, and A.L. Qualls. In situ thermal conductivity measurement of ceramics in a fast neutron environment. *Journal of Nuclear Materials*, Vol. 283-287, pp. 545–550, 2000.

[17] K. Yasuda, K. Tanaka, M. Shimada, T. Yamamoto, S. Matsumura, and C. Kinoshita. Influence of an electric field on the microstructure evolution of ion-irradiated alumina. *Journal of Nuclear Materials*, Vol. 329-333, pp. 1451–1455, 2004.

[18] W.J. Parker, R.J. Jenkis, C.P. Butler, and G. L. Abbott. Flash method of determining thermal diffusivity, heat capacity, and thermal conductivity. *Journal of Applied Physics*, pp. 1679–1684, 1961.

[19] M. Akiyoshi, N. Akasaka, Y. Tachi, and T. Yano. Interstitial atom behavior in neutron-irradiated beta-silicon nitride. *Journal of the Ceramic Society of Japan*, Vol. 112, No. 5, pp. 1490–1494, 2004.

[20] M. Akiyoshi, N. Akasaka, Y. Tachi, and T. Yano. Relation between macroscopic length change and the crystal structure in heavily neutron-irradiated ceramics. *Journal of Nuclear Materials*, Vol. 329-333, pp. 1466–1470, 2004.

[21] H. Miyazaki, T. Suzuki, T. Yano, and T. Iseki. Effect of thermal annealing on the macroscopic dimension and lattice parameter of heavily neutron-irradiated silicon carbide. *Journal of Nuclear Science and Technology*, Vol. 29, No. 7, pp. 656–663, July 1992.

[22] T. Yano, K. Sasaki, T. Maruyama, T. Iseki, M. Ito, and S. Onose. A step-heating dilatometry method to measure the change in length due to annealing of a SiC temperature monitor. *Nuclear Technology*, Vol. 93, pp. 412–415, March 1991.

[23] P. Kirkegaard, J.V. Olsen, M. Eldrup, and N.J. Pedersen. Palsfit: A computer program for analysing positron lifetime spectra. Technical report, RisøDTU, February 2009. Risø-R-1652, ISBN 978-87-550-3691-8.

[24] Y. Kanechika, M. Azuma, and H. Fukushima. Optimum sintering conditions for optical properties of translucent aluminum nitride ceramics. *Chinese Science Bulletin*, Vol. 54, No. 5, pp. 842–845, 2009.

[25] M. Akiyoshi, T. Yano, and M. Jenkins. A new type of defect on $\{11\bar{2}0\}$ planes in β-Si_3N_4 produced by neutron irradiation. *Philosophical Magazine Letters*, Vol. 81, No. 4, pp. 251–258, 2001.

[26] M. Akiyoshi and T. Yano. Connection structures between type-I and type-II defect in neutron irradiated β-Si_3N_4. *Journal of Electron Microscopy*, Vol. 52, pp. 267–275, 2003.

[27] Q. Xu, T. Yoshiie, and M. Okada. Positron annihilation of vacancy-type defects in neutron-irradiated 4H-SiC. *Journal of Nuclear Materials*, Vol. 386-388, pp. 169–172, 2009.

[28] S. Dannefaer and D. Kerr. Positron annihilation investigation of electron irradiation-produced defects in 6H-SiC. *Diamond and Related Materials*, Vol. 13, No. 1, pp. 157–165, 2004.

[29] L. Henry, MF. Barthe, C. Corbel, P. Desgardin, G. Blondiaux, S. Arpiainen, and L. Liszkay. Silicon vacancy-type defects in as-received and 12-MeV proton-irradiated 6H-SiC studied by positron annihilation spectroscopy. *Physical Review B*, Vol. 67, No. 11, p. 115210, 2003.

[30] A. Polity, S. Huth, and M. Lausmann. Defect characterization in electron-irradiated 6H-SiC by positron annihilation. *Physical Review B*, Vol. 59, No. 16, pp. 10603–10606, 1999.

[31] A. Kawasuso, H. Itoh, N. Morishita, M. Yoshikawa, T. Ohshima, I. Nashiyama, S. Okada, H. Okumura, and S. Yoshida. Silicon vacancies in 3C-SiC observed by positron lifetime and electron spin resonance. *Applied Physics A - Materials Science & Processing*, Vol. 67, No. 2, pp. 209–212, 1998.

[32] A. Kawasuso, H. Itoh, T. Ohshima, K. Abe, and S. Okada. Vacancy production by 3 MeV electron irradiation in 6H-SiC studied by positron lifetime spectroscopy. *Journal of Applied Physics*, Vol. 82, No. 7, pp. 3232–3238, 1997.

[33] A. Kawasuso, H. Itoh, S. Okada, and H. Okumura. Annealing processes of vacancy-type defects in electron-irradiated and as-grown 6H-SiC studied by positron lifetime spectroscopy. *Journal of Applied Physics*, Vol. 80, No. 10, pp. 5639–5645, 1996.

[34] T. Iwai, Y. Ito, and M. Koshimizu. Vacancy-type defect production in iron under ion beam irradiation investigated with positron beam Doppler broadening technique. *Journal of Nuclear Materials*, Vol. 329-333 Part2, pp. 963–966, 2004.

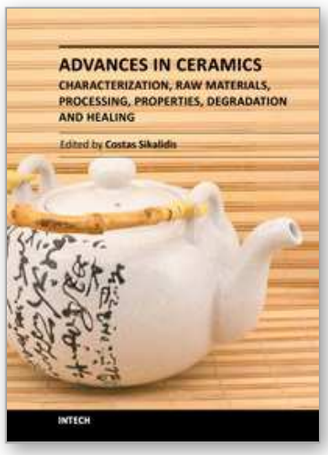

Advances in Ceramics - Characterization, Raw Materials, Processing, Properties, Degradation and Healing
Edited by Prof. Costas Sikalidis

ISBN 978-953-307-504-4
Hard cover, 370 pages
Publisher InTech
Published online 01, August, 2011
Published in print edition August, 2011

The current book consists of eighteen chapters divided into three sections. Section I includes nine topics in characterization techniques and evaluation of advanced ceramics dealing with newly developed photothermal, ultrasonic and ion spattering techniques, the neutron irradiation and the properties of ceramics, the existence of a polytypic multi-structured boron carbide, the oxygen isotope exchange between gases and nanoscale oxides and the evaluation of perovskite structures ceramics for sensors and ultrasonic applications. Section II includes six topics in raw materials, processes and mechanical and other properties of conventional and advanced ceramic materials, dealing with the evaluation of local raw materials and various types and forms of wastes for ceramics production, the effect of production parameters on ceramic properties, the evaluation of dental ceramics through application parameters and the reinforcement of ceramics by fibers. Section III, includes three topics in degradation, aging and healing of ceramic materials, dealing with the effect of granite waste addition on artificial and natural degradation bricks, the effect of aging, micro-voids, and self-healing on mechanical properties of glass ceramics and the crack-healing ability of structural ceramics.

How to reference
In order to correctly reference this scholarly work, feel free to copy and paste the following:

Masafumi Akiyoshi, Hidetsugu Tsuchida and Toyohiko Yano (2011). Thermal Diffusivity of Ceramics During Neutron Irradiation, Advances in Ceramics - Characterization, Raw Materials, Processing, Properties, Degradation and Healing, Prof. Costas Sikalidis (Ed.), ISBN: 978-953-307-504-4, InTech, Available from: http://www.intechopen.com/books/advances-in-ceramics-characterization-raw-materials-processing-properties-degradation-and-healing/thermal-diffusivity-of-ceramics-during-neutron-irradiation

INTECH
open science | open minds

InTech Europe
University Campus STeP Ri
Slavka Krautzeka 83/A
51000 Rijeka, Croatia
Phone: +385 (51) 770 447
Fax: +385 (51) 686 166
www.intechopen.com

InTech China
Unit 405, Office Block, Hotel Equatorial Shanghai
No.65, Yan An Road (West), Shanghai, 200040, China
中国上海市延安西路65号上海国际贵都大饭店办公楼405单元
Phone: +86-21-62489820
Fax: +86-21-62489821

IntechOpen